Non-hydrostatic modelling with the COSMO model

Michael Baldauf

Deutscher Wetterdienst, Germany
Offenbach, Germany
michael.baldauf@dwd.de

1 Introduction

The current NWP model chain of the DWD (Deutscher Wetterdienst) consists of the hydrostatic global model GME with a horizontal grid spacing of about 30 km, and two versions of the non-hydrostatic, compressible model COSMO: the COSMO-EU covering most parts of Europe with 7 km grid spacing and the convection-resolving COSMO-DE (2.8 km).

In particular both versions of the COSMO model use the Runge-Kutta (RK) integration scheme for the solution of the Euler equations, originally developed for the WRF model (Wicker and Skamarock, 2002). Their 3-stage Runge-Kutta scheme (denoted here as RK3WS) is extended by an implicit vertical advection calculation in the following manner (Baldauf et al., 2010). Starting from the fields Φ^n at time step n, first the implicit scheme for $\tilde{\Phi}$ is solved

$$\underbrace{\frac{\tilde{\Phi}-\Phi^n}{\frac{\Delta t}{3}}}_{=:L(\Phi^n)} = \beta A_z(\tilde{\Phi}) + (1-\beta)A_z(\Phi^n) + A_\lambda(\Phi^n) + A_\varphi(\Phi^n) + P(\Phi^n). \tag{1}$$

A_λ and A_φ are spatial discretisations of the horizontal advection in λ- and φ-direction (see eq. (12)). A_z denotes a vertical advection spatial operator. $P(\Phi^n)$ contains the tendencies of the physical parameterisations which are calculated once outside of the RK-scheme. Then the first RK-substep with the tendency $L(\Phi^n)$ is performed

$$\Phi^* = \Phi^n + \frac{\Delta t}{3} L(\Phi^n) \tag{2}$$

and the fast parts are calculated with tendency $(\Phi^* - \Phi^n)/(\Delta t/3)$, starting at Φ^n. The result is a new state Φ^*. In the second step

$$\underbrace{\frac{\tilde{\Phi}-[\alpha\Phi^n+(1-\alpha)\Phi^*]}{\frac{\Delta t}{2}}}_{=:L(\Phi^*)} = \beta A_z(\tilde{\Phi}) + (1-\beta)A_z(\Phi^*) + A_\lambda(\Phi^*) + A_\varphi(\Phi^*) + P(\Phi^n). \tag{3}$$

is solved and used for the RK-substep

$$\Phi^{**} = \Phi^n + \frac{\Delta t}{2} L(\Phi^*). \tag{4}$$

Then the fast waves with tendency $(\Phi^{**} - \Phi^n)/(\Delta t/2)$ are calculated starting at Φ^n giving a new state Φ^{**}. In the third step we solve

$$\underbrace{\frac{\tilde{\Phi}-[\alpha\Phi^n+(1-\alpha)\Phi^{**}]}{\Delta t}}_{=:L(\Phi^{**})} = \beta A_z(\tilde{\Phi}) + (1-\beta)A_z(\Phi^{**}) + A_\lambda(\Phi^{**}) + A_\varphi(\Phi^{**}) + P(\Phi^n). \tag{5}$$

leading to the third RK-substep

$$\Phi^{n+1} = \Phi^n + \Delta t\, L(\Phi^{**}). \tag{6}$$

Finally the fast waves with tendency $(\Phi^{n+1} - \Phi^n)/(\Delta t)$ are calculated starting at Φ^n which gives Φ^{n+1}. The overdamping weight α is equal to 0 in the original scheme of Wicker and Skamarock (2002). Unfortunately this limits the stability range of our vertical implicit advection scheme. A certain stabilisation can be achieved by the use of $\alpha = 1$.

The paper is split into two parts. The second section addresses the issue of stability of the RK time-splitting scheme. To this purpose a complete time *and* space von Neumann analysis of the above scheme is performed. The third section addresses a special issue of accuracy, namely the influence of the prominent stabilising damping mechanism (divergence damping) or the influence of several anelastic approximations of the basic equations compared to the correct solution.

2 Stability analysis

In the following a von Neumann stability analysis of the two-dimensional (2D), non-hydrostatic, compressible Euler equations

$$\frac{\partial u}{\partial t} + U_0 \frac{\partial u}{\partial x} = -\frac{1}{\rho_0}\frac{\partial p'}{\partial x} + \alpha_D \frac{\partial D}{\partial x}, \tag{7}$$

$$\frac{\partial w}{\partial t} + U_0 \frac{\partial w}{\partial x} = -\frac{1}{\rho_0}\frac{\partial p'}{\partial z} + g\left(\frac{T'}{T_0} - \frac{p'}{p_0}\right) + \alpha_D \frac{\partial D}{\partial z} \tag{8}$$

$$\frac{\partial p'}{\partial t} + U_0 \frac{\partial p'}{\partial x} = -\frac{c_p}{c_v} p_0 D + \rho_0 g w, \tag{9}$$

$$\underbrace{\frac{\partial T'}{\partial t} + U_0 \frac{\partial T'}{\partial x}}_{-\mathscr{P}_A} = \underbrace{-\frac{R}{c_v} T_0 D}_{\mathscr{P}_S} \underbrace{- \frac{\partial T_0}{\partial z} w}_{\mathscr{P}_B}, \underbrace{\qquad}_{\mathscr{P}_D} \tag{10}$$

with the divergence

$$D = \frac{\partial u}{\partial x} + \frac{\partial w}{\partial z} \tag{11}$$

is performed (more details can be found in Baldauf (2010)). Here terms are grouped as indicated into the processes 'advection' $\mathscr{P}_A$, 'sound propagation' $\mathscr{P}_S$, 'buoyancy' $\mathscr{P}_B$, and a possible artificial divergence damping term $\mathscr{P}_D$. This vertical slice model contains the most important features that restrict the stability of spatial and temporal discretisation schemes of a nonhydrostatic 3D-model applied to the convection permitting scale.

The only 'slow' process in these equations is the horizontal advection, for which a fifth order upwind scheme is used, e.g. in x-direction

$$A_j(\phi) = -U_0 \frac{-3\phi_{j+2} + 30\phi_{j+1} + 20\phi_j - 60\phi_{j-1} + 15\phi_{j-2} - 2\phi_{j-3}}{60\,\Delta x}. \tag{12}$$

A discussion of stability properties of several advection terms with a comprehensive theory of RK-schemes can be found in Baldauf (2008). Table (1) shows the *efficient* Courant number $C_{eff} := C/s$ (defined in Ruuth and Spiteri (2004)), where C means the maximum allowable Courant number (e.g. 1.42 for a 3-stage RK and an upwind 5th order scheme). The columns denote advection operators of several orders (upwind 1st, 3rd and 5th order or centred differences 2nd, 4th or 6th order). The rows denote the stage s of the RK-scheme (or more precisely: a certain subset of s-stage RK-schemes, called LC-RK in Baldauf (2008)). C_{eff} therefore takes into account the number of substeps needed for the calculation and consequently is a rough measure about the efficiency of the method. Apart from the low

	up1	cd2	up3	cd4	up5	cd6
LC-RK1	1	0	0	0	0	0
LC-RK2	0.5	0	0.437	0	0	0
LC-RK3	0.419	0.577	0.542	0.421	0.478	0.364
LC-RK4	0.348	0.707	0.436	0.515	0.433	0.446
LC-RK5	0.322	0	0.391	0	0.329	0
LC-RK6	0.296	0	0.385	0	0.311	0
LC-RK7	0.282	0.252	0.369	0.184	0.323	0.159

Table 1: The 'effective Courant number' $C_{eff} := C_{crit}/N$ for several upwind (up) and centred difference (cd) advection schemes and RK-schemes of different stages.

order advection schemes the most efficient combinations are RK3/upwind3, RK3/upwind5 (proposed by Wicker and Skamarock (2002) and also used in COSMO), and RK4/centred difference4.

All of the fast processes are spatially discretized by centred differences of 2nd order on a staggered grid in space. The temporal discretisation uses a forward-backward scheme in horizontal direction and an implicit (Crank-Nicholson) scheme in the vertical.

For the buoyancy terms alone (i.e. only the process $\mathscr{P}_B$ is considered) this leads to

$$\begin{aligned}
\frac{w^{n+1}-w^n}{\Delta t} &= g\left(\beta^B M_z \frac{T'^{n+1}}{T_0} + (1-\beta^B) M_z \frac{T'^n}{T_0} - \beta^B M_z \frac{p'^{n+1}}{p_0} - (1-\beta^B) M_z \frac{p'^n}{p_0}\right), \\
\frac{p'^{n+1}-p'^n}{\Delta t} &= \rho_0 g \left(\beta^B M_z w^{n+1} + (1-\beta^B) M_z w^n\right), \\
\frac{T'^{n+1}-T'^n}{\Delta t} &= -\frac{\partial T_0}{\partial z}\left(\beta^B M_z w^{n+1} + (1-\beta^B) M_z w^n\right).
\end{aligned}$$

which is unconditionally stable for the off-centring parameter $\beta^B \leq 1/2$ (M_z denotes a vertical averaging operator).

In the same manner for the sound terms alone (i.e. if only the process $\mathscr{P}_S$ is considered) such a discretisation is unconditionally stable for all vertical sound Courant numbers $C_{snd,z} = c_s \Delta t/\Delta z$ and horizontal numbers $C_{snd,x} = c_s \Delta t/\Delta x \leq 1$, (with the sound speed $c_s = (c_p/c_v \cdot RT_0)^{1/2}$) if the off-centring parameter of the Crank-Nicholson $\beta^s \geq 1/2$. ($\beta^s = 0$ means a purely explicit, $\beta^s = 0$ a purely implicit scheme).

A stability reduction arises, if these fast processes are combined with the advection via the RK time splitting procedure. For example if one combines only sound processes with the advection, then most of the waves are unstable for $\beta^s = 1/2$, even for moderate (and theoretically stable) values for $C_{adv}, C_{snd,x}$. But even for stronger off-centring (e.g. $\beta^s = 0.7$), horizontally propagating waves remain unstable. A solution for this problem is known since a long time (e.g. Skamarock and Klemp, 1992): the addition of an artificial divergence damping term $\mathscr{P}_D$ can stabilise all the waves of this linear 2D sound-advection system (even for $\beta^s = 1/2$).

But the inclusion of buoyancy effects destabilises the scheme to a very small extent: Figure 1 shows the maximum amplification factor λ_{max} (i.e. the maximum value over all wavevectors) in dependence on $C_{snd,x}$ and C_{adv} for different off-centrings β^B. One recognises that an optimal value is $\beta_B \approx 0.7$; higher values do not significantly increase the stability. Nevertheless a very slight instability remains. However it seems to be not relevant for weather prediction purposes or for climate runs of a limited area model, in which amplified perturbations are transported through the boundaries before disturbing the solution. One should remark that an increase of β^S does not improve the stability. However, a slightly higher value (e.g. $\beta^s = 0.7$) can stabilise the discretisation of the sound processes in steeper terrain

(this is not inspected here). It should be mentioned that for the strength of the divergence damping a value of $C_{div} := \alpha_D \Delta t/\Delta x^2 = 0.1$ was found to be necessary. For the COSMO-DE setting Δx =2.8 km and $\Delta t \approx$= 5 sec. this leads to $\alpha_D/c_s^2/\Delta t \approx 0.3$ which is larger than the value 0.1 recommended by Wicker and Skamarock (2002).

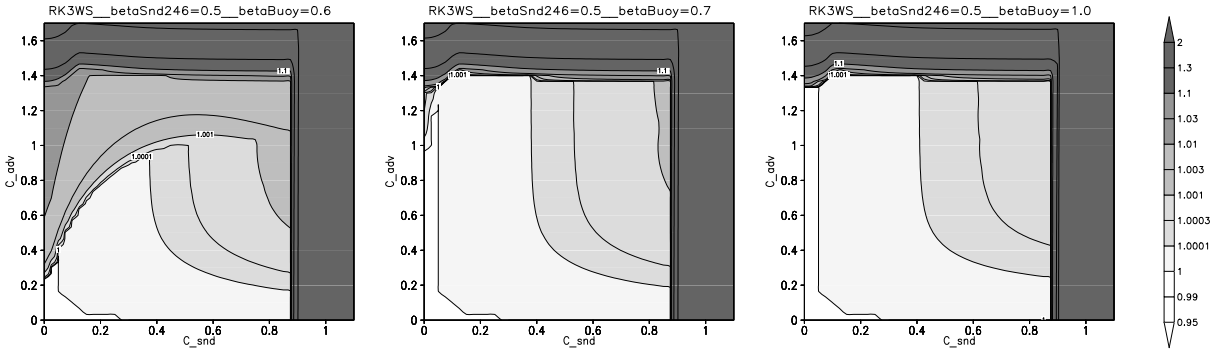

Figure 1: Maximum amplification factor λ_{max} in dependence on $C_{snd,x}$ and C_{adv} for RK3WS with advection, sound, buoyancy and divergence damping $C_{div,x} = 0.1$ for different off-centring for buoyancy $\beta^B = 0.6, 0.7, 1.0$. Sound off-centring-coefficient is $\beta^s = 1/2$ (i.e. trapezoidal). Time-integration scheme RK3WS, White colour means stable range ($\lambda_{max} \leq 1$), Isolines are at 1.0, 1.0001, 1.0003, 1.001, 1.003, 1.01, ...

A further look at table 1 shows that the combination of a 4-stage, 2nd order RK scheme (called RK4MS)

$$q^{(1)} = q^n + \frac{1}{4}\Delta t\ f(q^n), \tag{13}$$

$$q^{(2)} = q^n + \frac{1}{3}\Delta t\ f(q^{(1)}), \tag{14}$$

$$q^{(3)} = q^n + \frac{1}{2}\Delta t\ f(q^{(2)}), \tag{15}$$

$$q^{n+1} = q^n + \Delta t\ f(q^{(3)}), \tag{16}$$

and the centred difference 4th order advection operator gives a pretty large stable Courant number $C_{adv} =$ 2.06 leading to the large effective Courant number $C_{eff} = 0.515$. Therefore one can expect that the time-split scheme will be efficient. The large allowable large time-step overcompensates the additional RK substep (compared to the 3-stage RK). Figure 2 shows the amplification factor for this scheme. Due to the fact that a centred difference advection scheme is used, short waves reduce the stability of the scheme (top, left figure). A weak additional 4th order smoothing (with a diffusion coefficient $K = C_{smo}\Delta x^4/\Delta t$) damps these short waves and results in a quite stable scheme. Again a more elaborate analysis can be found in Baldauf (2010).

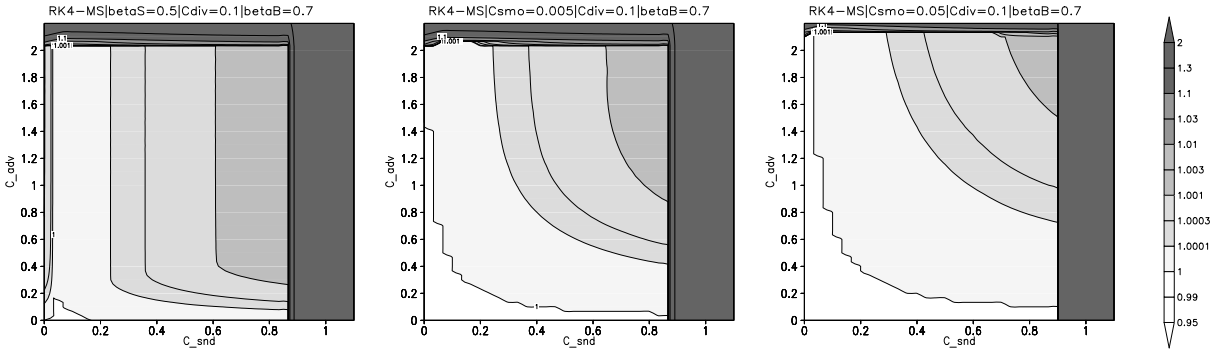

Figure 2: λ_{max} for RK4MS with cd4 advection, $C_{div,x} = 0.1$, with different smoothing $C_{smo} = 0, 0.005, 0.05$.

3 Normal mode analysis

Numerical stability is one of the most important properties of a dynamical core. Another important aspect is accuracy. This can be analysed by the calculation of truncation errors or by performing idealised tests with known solutions. In the following we want to highlight the role of the artificial divergence damping by answering the question in which sense it perturbs linear properties (wave expansion). This will be done on the level of the analytic equations. The resulting normal mode analysis can be quite easily extended to the consideration of some anelastic approximation sets (Ogura and Phillips (1962), here denoted as 'OP62', Wilhelmson and Ogura (1972), 'WO72', and Lipps and Hemler (1982), 'LH82'). These approximations are of interest for COSMO because in a current project possible benefits of the EULAG dynamical core (e.g. Smolarkiewicz and Prusa, 2005) are inspected. The basic ideas follow the normal mode analysis of Davies et al. (2003).

In the following a steady atmosphere (no base flow $u_0 = 0$) is assumed. We will use an equation for the pressure perturbation p' as in the COSMO-model, but a continuity equation to have a direct control about the anelastic approximations. The appropriate linearised equations read

$$\frac{\partial u'}{\partial t} = -\frac{1}{\rho_0}\frac{\partial p'}{\partial x} + fv' + \alpha_D \frac{\partial D'}{\partial x} \tag{17}$$

$$\frac{\partial v'}{\partial t} = -\frac{1}{\rho_0}\frac{\partial p'}{\partial y} - fu' + \alpha_D \frac{\partial D'}{\partial y} \tag{18}$$

$$\delta_1 \frac{\partial w'}{\partial t} = -\frac{1}{\rho_0}\frac{\partial p'}{\partial z} - \delta_{LH}\frac{1}{\rho_0}\frac{N^2}{g}p' - g\frac{\rho'}{\rho_0} + \alpha_D \frac{\partial D'}{\partial z} \tag{19}$$

$$\delta_2 \frac{\partial \rho'}{\partial t} + w'\frac{\partial \rho_0}{\partial z} = -\rho_0 D' \tag{20}$$

$$\frac{\partial p'}{\partial t} + \underbrace{w'\frac{\partial p_0}{\partial z}}_{=-g\rho_0 w'} = c_s^2\left(\frac{\partial \rho'}{\partial t} + w'\frac{\partial \rho_0}{\partial z}\right) \tag{21}$$

$$D' := \frac{\partial u'}{\partial x} + \frac{\partial v'}{\partial y} + \frac{\partial w'}{\partial z}. \tag{22}$$

Some switches were introduced whose values (0 or 1) are summarised in table 2. $\delta_1 = 0$ delivers the hydrostatic approximation, and δ_2 is the main switch of the anelastic approximation. The additional term $\sim \delta_{LH}$ only arises in the equation system of LH82[1]. This is the only difference toward OP62 or WO72; the continuity equation is the same for all of the three anelastic equation sets, and the pressure equation is just the linearised adiabatic state equation $d\Theta/dt = 0$ used by them, too. Furthermore, it should be mentioned that in this *linear* analysis there is no difference between the equation systems of OP62 and WO72.

equation system	δ_1	δ_2	δ_{LH}	α_D
compressible	1	1	0	0
compressible, with div. damping	1	1	0	$\neq 0$
anelastic (OP62, WO72)	1	0	0	0
anelastic (LH82)	1	0	1	0

Table 2: Switches for the different equation sets inspected in the normal mode analysis.

The coefficient functions of the linearised equations (17)-(22) are dependent on z. To reduce this z-

[1] For the pressure gradient and the buoyancy term LH82 use $-c_p\nabla\Theta_0\pi' + \mathbf{g}\Theta'/\Theta_0$ instead of the correct term $-c_p\Theta\nabla\pi' + \mathbf{g}\Theta'/\Theta_0$ (Nance and Durran, 1994). In linear approximation the difference between these two terms is $-c_p\pi'\nabla\Theta_0$. Expressed by the variables used in the equation system above this can be approximated linearly by $-\frac{1}{\rho_0}\frac{N^2}{g}p'$.

dependency (the following Fourier transformation requires even constant coefficients) we perform a variable transformation by a function of the density according to Bretherton (1966, section 5):

$$\phi' = \left(\frac{\rho_0}{\rho_s}\right)^{\alpha} \cdot \phi_b. \tag{23}$$

where ρ_s is a constant reference value (e.g. at the bottom). The exponent is $\alpha = -1/2$ for $\phi' = u$, v, w, T' and $\alpha = +1/2$ for $\phi' = p'$, ρ'. Insertion into eqns. (17)-(22) results in a quite similar system with additional terms proportional to the (inverse) scale height

$$\delta := -\frac{\partial}{\partial z}\left(\log\frac{\rho_0}{\rho_s}\right). \tag{24}$$

In the special case of an isothermal atmosphere ($T_0 = const.$) the density is purely exponential and therefore $\delta = g/(RT_0) = const$. The result of this Bretherton transformation is that some coefficients (namely those $\sim 1/\rho_s$) become constant, whereas others like $\sim c_s^2$, $\sim T_0$, $\sim \delta$ remain dependent on z (they are only constant for an isothermal atmosphere). But this z-dependency is quite weak, therefore they can also be considered nearly as constant. This allows to extent the analysis to more realistic stratifications (see 'second stratification case' below).

It is convenient to introduce the acoustic cutoff frequency

$$\omega_a^2 = N^2 + \frac{g^2}{c_s^2} \tag{25}$$

with the Brunt-Väisälä-frequency

$$N^2 = \frac{g}{\Theta_0}\frac{\partial\Theta_0}{\partial z} = \frac{g}{T_0}\left(\frac{\partial T_0}{\partial z} + \frac{g}{c_p}\right). \tag{26}$$

With the aid of the sound velocity, the ideal gas equation and the hydrostatic equation one can derive

$$\omega_a^2 = -\frac{g}{\rho_0}\frac{\partial\rho_0}{\partial z} \tag{27}$$

and therefore $\delta = \omega_a^2/g$.

Now we can Fourier transform the equations by

$$\phi_b'(x,y,z,t) = \hat{\phi}_b(k_x,k_y,k_z,\omega)\, e^{i(k_x x + k_y y + k_z z - \omega t)}. \tag{28}$$

This leads to a system of the form $\mathbf{A}\cdot(\hat{u}_b,\hat{v}_b,\hat{w}_b,\hat{\rho}_b,\hat{p}_b)^T = 0$ with

$$\mathbf{A} = \begin{pmatrix} i\omega + \alpha_D(ik_x)^2 & f - \alpha_D k_x k_y & \alpha_D ik_x(ik_z + \frac{\delta}{2}) & 0 & -ik_x\frac{1}{\rho_s} \\ -f - \alpha_D k_x k_y & i\omega + \alpha_D(ik_y)^2 & \alpha_D ik_y(ik_z + \frac{\delta}{2}) & 0 & -ik_y\frac{1}{\rho_s} \\ \alpha_D ik_x(ik_z + \frac{\delta}{2}) & \alpha_D ik_y(ik_z + \frac{\delta}{2}) & \delta_1 i\omega + \alpha_D(ik_z + \frac{\delta}{2})^2 & -\frac{g}{\rho_s} & A_{35} \\ -ik_x\rho_s & -ik_y\rho_s & \frac{\rho_s}{g}\omega_a^2 - (ik_z + \frac{\delta}{2})\rho_s & \delta_2 i\omega & 0 \\ 0 & 0 & -\frac{\rho_s}{g}N^2c_s^2 & -i\omega c_s^2 & i\omega \end{pmatrix} \tag{29}$$

with the abbreviation

$$A_{35} := -\left(ik_z - \frac{\delta}{2}\right)\frac{1}{\rho_s} - \delta_{LH}\frac{1}{\rho_s}\frac{N^2}{g}.$$

After an appropriate non-dimensionalization the requirement $\det A = 0$ leads to the characteristic equation for $\omega(\mathbf{k})$. This delivers the following dispersion relations:

The characteristic equation for the **non-hydrostatic, compressible equations** follows from the switches $\delta_1 = 1$, $\delta_2 = 1$, and $\delta_{LH} = 0$:

$$\omega^4 + \alpha_D \left(ik^2 - i\frac{1}{4}\delta^2 + k_z\delta \right) \omega^3 - \left(c_s^2 k^2 + \frac{1}{4}\frac{\omega_a^4}{\omega_a^2 - N^2} + f^2 \right) \omega^2$$
$$-\alpha_D f^2 \left(ik_z^2 - i\frac{1}{4}\delta^2 + k_z\delta \right) \omega + c_s^2(k_x^2 + k_y^2)N^2 + f^2 \left(c_s^2 k_z^2 + \frac{1}{4}\frac{\omega_a^4}{\omega_a^2 - N^2} \right) = 0 \qquad (30)$$

For $\alpha_D = 0$ we get the correct compressible solution whereas the influence of the artificial divergence damping can be inspected by $\alpha_D \neq 0$.

The different **anelastic approximations** follow from $\delta_1 = 1$, $\delta_2 = 0$ (and $\alpha_D = 0$). The equation sets of OP62 and WO72 are generated by $\delta_{LH} = 0$, those of LH82 by $\delta_{LH} = 1$. This results in the dispersion relation

$$\left[\frac{c_s^2}{\omega_a^2} k^2 + a_1 \right] \omega^2 - \left[\frac{c_s^2}{\omega_a^2}(k_x^2 + k_y^2)N^2 + f^2 \left(\frac{c_s^2}{\omega_a^2} k_z^2 + a_1 \right) \right] = 0 \qquad (31)$$

with

$$a_1 \quad := \quad 1 + (1 - \delta_{LH}) ik_z \frac{c_s}{\omega_a} \frac{n^2}{\sqrt{1 - n^2}} + \frac{1}{4}\frac{2n^2(1 + \delta_{LH}) - 3}{1 - n^2} \qquad (32)$$

and $n := N/\omega_a$. The anelastic approximation eliminates sound waves, only the two branches for gravity waves are contained. Purely horizontally propagating waves are undamped. A small damping occurs if the wave vector **k** has a vertical component, too.

Discussion of the results Two stratifications are considered. The first case is an isothermal atmosphere with $T_0 = 260$ K. In this case the inverse scale height is $\delta \approx 1/7606.5$ 1/m, $c_s \approx 323.2$ m/s, $N \approx 0.01919$ 1/s, and $\omega_a \approx 0.03591$ 1/s.

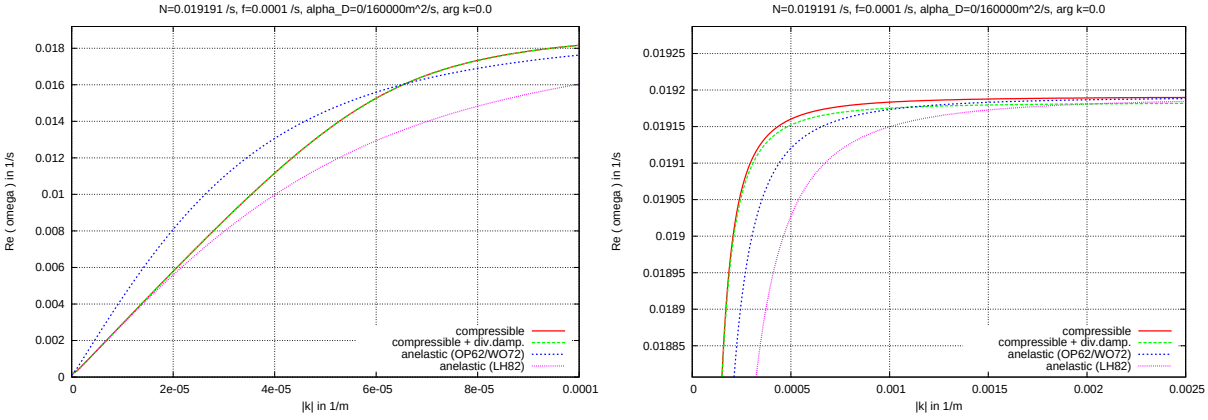

Figure 3: Dispersion relation for horizontally propagating gravity waves (i.e. $k_z = 0$) for the isothermal atmosphere ($T_0 = 260$ K, $f = 10^{-4}$ 1/s). Red: correct (compressible) solution, green: compressible equations with divergence damping, blue: OP62 approximation, magenta: LH82 approximation. Left: focus on long waves, right: focus on short waves.

The right panel of Fig. 3 shows the behaviour for short gravity waves ($k = 0.0025$ 1/m corresponds to a wavelength $\lambda = 2\pi/k \approx 2.5$ km). All the anelastic approximations are quite close to the correct solution $\omega \to N$ for $k \to \infty$. The compressible equations *with divergence damping* do not converge to this solution. But the deviations are less than about 0.05% and therefore are negligible.

The left panel of Fig. 3 focuses on long gravity waves ($k = 0.0001$ 1/m corresponds to a wavelength $\lambda \approx 63$ km). Obviously the divergence damping has no spurious influence on this type of waves. The OP62/WO72 approximations show stronger deviations from the true solution. The LH82 approximation represents very long waves with reasonable accuracy but strongly deviates for a medium range of wavelengths (even greater as for OP62/WO72). These results are in good quantitative agreement with Davies et al. (2003).

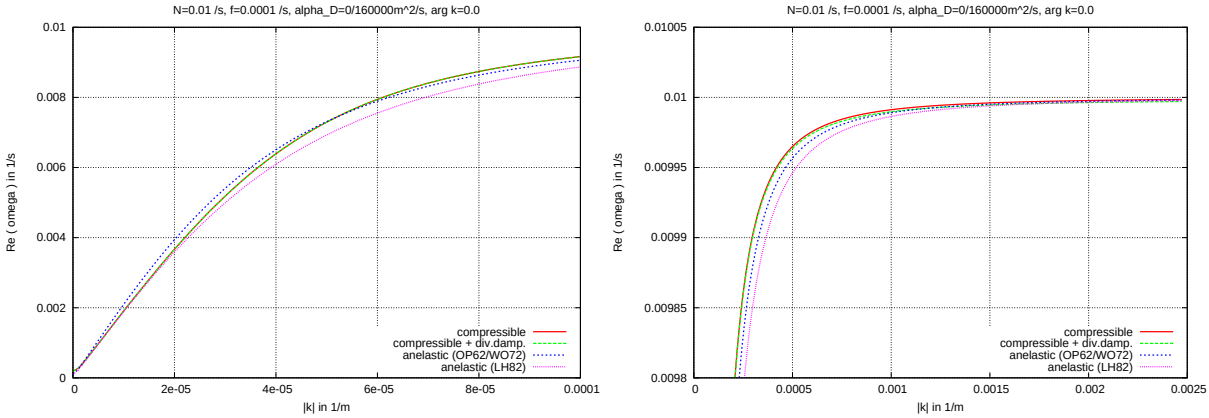

Figure 4: Dispersion relation for gravity waves as in Fig. 3 now for a 'standard atmosphere' ($N = 0.01$ 1/s, $f = 10^{-4}$ 1/s).

The second case is a standard atmosphere with $N = 0.01$ 1/s. By eq. (25) we can derive $\omega_a \approx 0.03196$ 1/s. Again a mean temperature of $T = 260$ K is assumed to estimate a mean $c_s = 323.2$ m/s. A comparison between this case (Fig. 4) and the isothermal case (Fig. 3) shows that the statements above about gravity waves in the isothermal case are qualitatively the same. But the quantitative deviations from the true solution are much smaller. E.g. the LH82 approximation deviates less than 4% from the true frequency, the OP62 approximation even less.

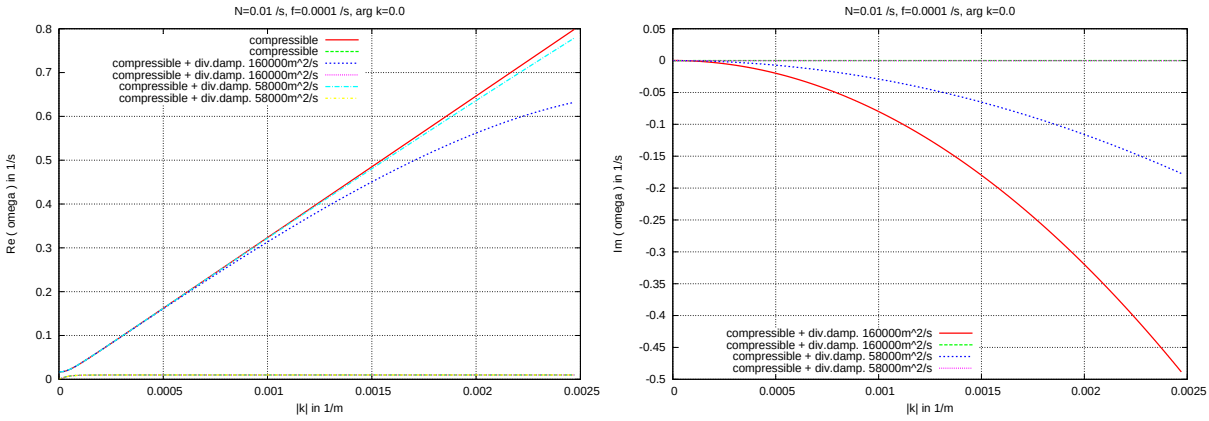

Figure 5: Dispersion relation for the compressible equations with/without divergence damping for a standard atmosphere $N = 0.01$ 1/s, $f = 10^{-4}$ 1/s, only horizontally propagating waves. Real part (left), colours for sound waves: red: correct solution, blue: $\alpha_D = 160000\ m^2/s$ (or $C_{div,x} = 0.1$), cyan: $\alpha_D = 58000\ m^2/s$ (or $C_{div,x} = 0.03$). Imaginary part (right) colours for sound waves: red: $\alpha_D = 160000\ m^2/s$ (or $C_{div,x} = 0.1$), blue: $\alpha_D = 58000\ m^2/s$ (or $C_{div,x} = 0.03$).

Finally we want to inspect the behaviour of sound waves for different strengths of the divergence damping. Fig. 5 (left) shows that only short sound waves differ in the real part of the dispersion relation toward the true solution. But the negative imaginary part shows a strong damping of these sound waves.

The influence of the stratification to sound waves is small as expected The appropriate figures for an isothermal stratification look rather similar (not shown).

To summarise, the normal mode analysis shows that divergence damping has no serious influence on the linear behaviour of the compressible equations. The anelastic approximations are applicable on smaller scales (e.g. regional of convection resolving scales). But they show some deviations for longer gravity waves, which seems to be severe only in the case of an isothermal atmosphere (which is a bit unrealistic for the whole troposphere).

References

Baldauf, M. (2008). Stability analysis for linear discretisations of the advection equation with Runge-Kutta time integration. *J. Comput. Phys. 227*, 6638–6659.

Baldauf, M. (2010). Linear stability analysis of Runge-Kutta based partial time-splitting schemes for the Euler equations. *Mon. Wea. Rev. 138*, 4475–4496.

Baldauf, M., A. Seifert, J. Förstner, D. Majewski, M. Raschendorfer, and T. Reinhardt (2010). Operational convective-scale numerical weather prediction with the COSMO model. *submitted to Mon. Wea. Rev.*.

Bretherton, F. P. (1966). The propagation of groups of internal gravity waves in a shear flow. *Quart. J. Roy. Met. Soc. 92*, 466–480.

Davies, T., A. Staniforth, N. Wood, and J. Thuburn (2003). Validity of anelastic and other equation sets as inferred from normal-mode analysis. *Quart. J. Roy. Met. Soc. 129*, 2761–2775.

Lipps, F. B. and R. S. Hemler (1982). A scale-analysis of deep moist convection and some related numerical calculations. *J. Atmos. Sci. 39*, 2192–2210.

Nance, L. B. and D. R. Durran (1994). A comparison of the accuracy of three anelastic systems and the pseudo-incompressible system. *JAS 52*(24), 3549–3565.

Ogura, Y. and N. A. Phillips (1962). Scale analysis of deep and shallow convection in the atmosphere. *J. Atmos. Sci. 19*, 173.

Ruuth, S. J. and R. J. Spiteri (2004). High-Order Strong-Stability-Preserving Runge-Kutta Methods with downwind-biased spatial Discretizations. *SIAM J. Numer. Anal. 42*(3), 974–996.

Skamarock, W. C. and J. B. Klemp (1992). The stability of time-split numerical methods for the hydrostatic and the nonhydrostatic elastic equations. *Mon. Wea. Rev. 120*, 2109–2127.

Smolarkiewicz, P. K. and J. M. Prusa (2005). Towards mesh adaptivity for geophysical turbulence: continuous mapping approach. *Int. J. Numer. Meth. Fluids 47*, 789–801.

Wicker, L. J. and W. C. Skamarock (2002). Time Splitting Methods for Elastic Models using Forward Time Schemes. *Mon. Wea. Rev. 130*, 2088–2097.

Wilhelmson, R. and Y. Ogura (1972). The pressure perturbation and the numerical modeling of a cloud. *J. Atmos. Sci. 29*, 1295–1307.